Crack velocity jumps engendered by a transformational process zone

A. Boulbitch[1] and A. L. Korzhenevskii[2]
[1]*IEE S.A. ZAE Weiergewan, 11, rue Edmond Reuter, L-5326 Contern, Luxembourg*
[2]*Institute for Problems of Mechanical Engineering, RAS, Bol'shoi prosp. V. O. 61, 199178 St. Petersburg, Russia*
(Received 24 October 2015; published 7 June 2016)

We study a concerted propagation of a fast crack with the process zone where a rearrangement of the solid structure takes place. The latter is treated as a second-order local phase transformation. We demonstrate that the propagation of such a zone gives rise to a nonlinear frictionlike force exerted on the crack tip, resisting its propagation. Depending on the temperature, it produces three regimes of crack motion, which differ in the behavior of the crack tip process zone: (i) always existing, (ii) only emerging at a high crack speed, and (iii) flickering. We show that the latter regime exhibits crack velocity jumps.

DOI: 10.1103/PhysRevE.93.063001

I. INTRODUCTION

The speed, V, of a brittle crack has long been believed to be a continuous, monotonic function of the driving force G [1]. In contradiction to the above picture, experiments have recently revealed a fast crack propagation [2] exhibiting a terminal crack speed considerably lower than the Rayleigh velocity [2,3]. In addition, discontinuities in the dependence of the crack velocity on the driving force have been recently observed in materials as different as silicon [4,5] and limestone [6]. Until now, no explanation of these discontinuities has been available. Here we argue that this behavior can be generated by a transformational process zone (PZ).

A common opinion exists that the crack behavior is determined by the PZ, a nano- to meso-sized domain in the vicinity of its tip. For a long time, the structure of the PZ was beyond the reach of experiments. Recently, however, new experimental techniques have changed this situation. Traditional indirect methods are now being replaced by others that make it possible to obtain the PZ structure with a high spatial resolution, usually combining several techniques in one investigation. These recent techniques are often appropriate for propagating cracks. High-angle annular dark-field scanning transmission electron miroscopy (TEM) presently allows the direct imaging of atomic locations [7]. It can be combined with electron nanodiffraction [8]. A micromechanical loading has been combined with *in situ* high-resolution x-ray microdiffraction [9], and *in situ* scanning electron microscopy (SEM) has been combined with electron backscatter diffraction [10]. One used an *in situ* optical correlation technique [11] combined with Raman mapping [12]. Atomic force microscopy allows one to map the spontaneous strain [13,14]. Nanoindentation makes it possible to study the temperature dependence of the size of the PZ [15].

The emergence of the notion of the process zone reflects the understanding that a small domain in the immediate vicinity of the crack tip has specific properties that differ from those of the bulk of the solid. The PZ can only be distinguished from the rest of the solid if at least one of its physical properties varies perceptibly across its boundary. This may be an abrupt quantitative change, such as a steep growth of the elastic nonlinearity [16] or hyperelasticity [17] at the tip. Much more probable is, however, a qualitative change. In the latter case, the PZ differs from the bulk by, e.g., its chemical composition, electronic properties (such as, e.g., metal-isolator or exciton condensate-exciton gas), or crystal structure.

We focus here on the case in which the PZ and the bulk differ qualitatively, the difference being parametrized by a field, $\eta = \eta(\mathbf{r},t)$, referred to as the "order parameter." Without loss of generality, one may assume that $\eta \neq 0$ inside the PZ, while vanishing outside. In this respect, our approach is akin to the theory of phase transitions [18] as well as to the popular phase-field approach [19].

The terms "phase transition" and "order parameter" pertain equally to indicate a variation in the crystal structure in solids and bifurcations in nonlinear systems, both equilibrium and nonequilibrium, such as, e.g., bifurcations taking place during chemical reactions [20]. This implies that each of these transitions can be described by its order parameter, the inherent degree(s) of freedom responsible for the bifurcation or for the structural variation.

With respect to the formation of the PZ, all order parameters split into two classes. An order parameter belonging to the first class is conjugate to the strain tensor, $\varepsilon = \varepsilon(\mathbf{r})$. This means that under the action of the solid symmetry group, the order parameter η transforms as the strain tensor ε or as some of its components. In the theory of phase transitions, this case is classified as "proper ferroelastic." In this case, the equation for the order parameter admits an absolute term $\sim\varepsilon$ [21]. The latter gives rise to the PZ existing at any value of the temperature and stress intensity. Far from the tip, such an order parameter has the asymptotics $\eta \sim \varepsilon(\mathbf{r})$. The crystal structure of such a zone can be obtained from that of the bulk by superimposing a certain strain representing the order parameter.

The second class unifies those solids for which symmetry prohibits the order parameter's being conjugate to the strain tensor. Unlike the first class case, the crystal symmetry here cannot be obtained from the bulk symmetry distorted by a strain. In this case, the strain has an indirect effect on the order parameter: the PZ only emerges as soon as certain thermodynamic conditions are met. In other words, the behavior of the PZ exhibits features of a bifurcation.

Such a classification can be applied to the cases with a group-subgroup relation between the PZ and matrix symmetries or if the PZ and the matrix symmetries are subgroups of a common group. Transitions referred to as "reconstructive" exhibit no such relations and require a special modification of the Landau theory [22]. In particular, the family of martensitic transformations occupies a position intermediate between these two classes. On the one hand, the symmetry changes

during such transformations are described by the so-called "transcendental" order parameters, differing from a strain [23]. On the other hand, the transitions are accompanied by spontaneous strains which are typically large, admitting an approximate treatment of the problem similar to that in proper ferroelastics [24].

Transformational PZs of the second kind have been observed in many materials. Ferro- [25] and antiferroelectric ceramics [12] exhibit local phase transitions (LPTs) at the crack tips with the polarization playing the role of the order parameter in the former case and the optical phonon amplitude in the latter. Superconductive yttrium barium copper oxides and bismuth stronium calcium copper oxides [26] exhibit superconducting LPT at the tip, described by the order parameter representing the condensate wave function. Formation of hydride at the crack tip has been observed in the ZrNb alloy [27], where the order parameter describes the hydride number density. Structural rearrangement within the crack tip zone has been recently reported in sapphire [28]. Transformational PZs have also been reported in polymers [29]. Crack tip induced crystallization of the amorphous material has been observed in metallic glass Zr-Al-Ti-Cu-Ni alloy [30] as well as in resins, where it strongly affects the fracture process [31]. All these cases admit a description of the LPT by various order parameters η different from a strain.

In the theoretical description of the LPT, two strands of research can be pointed out. On the one hand, atomistic mechanisms of LPTs have been revealed by computer simulations and density-functional-theory-like calculations for several solids, such as iron [32–34], silicon [5,35,36], tantalum [37], zirconium [38], UO_2 [39], molybdenum [8], and Nitinol [40].

On the other hand, an analytical theory has been developed within a mechanical approach based on the assumption that the LPT zone only differs from the rest of the solid by (i) its elastic constants and (ii) spontaneous strain. Here we only cite a few such papers [41–47]. The transformation toughness mechanisms established up to now are static [48,49] or quasistatic and velocity independent [50]. In addition, they essentially require the presence of a metastable state. That is, they only work inside the two-phase region of the phase diagram, while vanishing outside.

In the present paper we develop an approach that differs from the above two. We address the stress-induced structural phase transformation related to the condensation of the optical phonons at the tip of a propagating crack described by the order parameters $\eta_i = \eta_i(\mathbf{r},t)$, subject to a specific equation of motion (the time-dependent Ginzburg-Landau equation), which determines their spatial distribution and dynamics. In other words, we study a transformational PZ of the second class, representing a phase localized at the crack tip and differing from the phase in the bulk of the solid.

Nabutovsky and Shapiro pioneered such an approach by describing an LPT generated by a dislocation [51]. This enabled revealing the effect of the local transition on the behavior of a dislocation and on the plastic properties of solids [52], describing the local phase formation at a propagating dislocation [53], as well as at wide [54] and narrow [55] domain walls and twin boundaries. The general properties of such a local phase formation have been described in Ref. [56].

The transformational PZ at the tip of a motionless crack within this approach has been analytically described in Refs. [56–58] and numerically addressed in Refs. [59] and [60].

A propagating crack with a transformational PZ at its tip has been recently studied in our papers [58,61,62]. We have described the formation of a transformational PZ at the tip of a propagating crack in the case of a second order [58,61] and a first order LPT [62]. We have demonstrated that the zone vanishes at high crack speeds [58]. We have further shown that the dynamics of the PZ order parameter strongly affects the motion of the crack, giving rise to a stick-slip instability during wedging [61] and limiting the terminal crack velocity [62].

Within linear elastic fracture mechanics, the classical uniform rectilinear crack propagation is described by Freund's equation [1]. In contrast, the description of the dynamics of a crack with a process zone at its tip requires an essential modification, taking into account the energy dissipation by the zone.

In the present paper we derive such an equation and describe a concerted motion of the crack with a transformational PZ. We show that the transformational PZ considerably alters the crack dynamics. We introduce a characteristic plane in terms of the temperature and the crack driving force and show that each specific regime of crack propagation defines a trajectory within this plane. We further determine the plane region where the process zone exists and explicitly find its boundary. For the first time, we show that the energy dissipation within the transformational PZ gives rise to the discontinuities in the $V = V(G)$ dependence as soon as the crack evolution trajectory crosses the boundary of the domain of existence of a PZ. We separate three possible regimes of crack propagation, differing in the number and positions of such $V = V(G)$ discontinuities.

In this paper we only focus on the second-order phase transition within the PZ. This enables us to perform a rigorous analytical analysis based on bifurcation theory and valid in the vicinity of the bifurcation boundary. This analysis is further supported by finite-element simulations valid also far from the bifurcation boundary. The first-order PZs will be addressed elsewhere.

This paper is organized as follows. In Sec. II we derive a general expression for the viscouslike friction force engendered by the internal dynamics within the propagating zone. We put forward a system of equations of motion describing the concerted propagation of the crack-PZ complex. For the convenience of the reader, a detailed description of the bifurcation is published separately [58] in a freely downloadable form. It contains a description of the internal dynamics of the PZ, as well as detailed discussions. In Sec. III we briefly summarize its results. In Sec. IV we derive the equation of motion of the crack and discuss the regimes of crack propagation following from its analysis. The latter is carried out in Appendix A. Section V describes our simulations, yielding a numerical solution of the concerted motion of the crack-PZ complex. A discussion and numerical estimates are given in Sec. VI.

Section VII summarizes our results. Appendix B contains technical details of our simulations.

II. FREE-ENERGY DISSIPATION RATE AND DISSIPATION-GENERATED CONFIGURATIONAL FORCE

In this section we derive a fundamental expression relating the viscous force resisting the crack propagation to the dissipation function of a system depending on the internal degrees of freedom exhibiting a dissipative dynamics.

Let us consider a solid with several internal degrees of freedom, such as optical and acoustic phonons, magnons, etc., n of them, η_i $(i = 1,2,\ldots,n)$, forming a macroscopic condensate. In its most general form, the free energy of this system can be written as

$$F = \int \Phi(\eta_i, \nabla\eta_i) d\Omega, \tag{1}$$

where η_i are referred to as the "order parameters," $\nabla\eta_i$ are their gradients, and Ω is the volume of the domain occupied by the system. The positively defined function, $\Phi = \Phi(\eta_i, \nabla\eta_i)$, is the mean-field free-energy density.

The kinetics of this system is controlled by the dissipative function, D [18]:

$$D = \frac{1}{2}\sum_{i=1}^{n}\int \kappa_i \left(\frac{\partial\eta_i}{\partial t}\right)^2 d\Omega, \tag{2}$$

where $\kappa_i > 0$ are the kinetic coefficients of the corresponding degrees of freedom and t is the time. It is assumed here that both (1) and (2) are written in terms of normal coordinates of the solid, which is always possible [18]. For this reason, the quadratic form (2) contains no offdiagonal terms. Let us note that generally the parameters κ_i are unequal to each other, unless this is required by symmetry.

The rate of the free-energy dissipation, $\partial F/\partial t$, is related to the dissipation function, D:

$$\frac{\partial F}{\partial t} = -2D \tag{3}$$

the relation (3) being exact [18].

Let us consider a PZ propagating together with the crack tip with the velocity V along the x axis. In a standard linear-viscous case one finds: $\partial F/\partial t = kV^2$, where k is a constant. One can then represent as $\partial F/\partial t = -fV$. Then the factor $f = kV$ is a linear viscous friction force. In general, $\partial F/\partial t$ may be a complex function of the velocity. Representing $\partial F/\partial t = -f(V)V$ one interprets the function $f(V)$ as a nonlinear viscous friction force. One concludes that the friction force applied to the crack tip has the form:

$$f = \frac{2D}{V}. \tag{4}$$

In the comoving frame, $x' = x - Vt$; $y' = y$, $\eta_i(x,y,t) = \eta_i(x',y')$ the dissipation function (2) takes the form:

$$D = \frac{V^2}{2}\sum_{i=1}^{n}\int \kappa_i \left[\frac{\partial\eta_i(\mathbf{r}')}{\partial x'}\right]^2 d\Omega, \tag{5}$$

where $\mathbf{r}' = (x',y')$ is the radius vector in the moving frame. Let us introduce the friction force (per unit crack length, L_z, in the Oz direction): $\Delta\Gamma = f/L_z$. Making use of the general relation (4), one finds the configurational friction force exerted on the crack tip:

$$\Delta\Gamma = V\sum_{i=1}^{n}\int \kappa_i \left(\frac{\partial\eta_i(\mathbf{r}')}{\partial x'}\right)^2 d^2r, \tag{6}$$

where the integration runs over the (x,y) plane.

The origin of this force can be made evident by the following arguments. Let us consider a point $\mathfrak{M}$ lying far away in front of the tip but close to its trajectory. At this point the order parameters initially have values close to zero $[\eta_i(r_{\mathfrak{M}}) \approx 0]$. As soon as the crack tip approaches this point, the order parameters increase, reach their maximum values $(\eta_i(\mathbf{r}_{\mathfrak{M}}) \neq 0)$, and vanish again after the tip has passed. The order parameters thus evolve over time, which is followed by a certain energy dissipation. It is this energy dissipation that gives rise to the friction force. It is worth noting that the configurational friction force (6) is nonlinear in the velocity, the nonlinearity being hidden in the dependence of the order parameters η_i on V.

One concludes that in order to calculate the friction force (6) one only needs to know the distribution, $\eta = \eta(\mathbf{r}')$, of the order parameter in the vicinity of the crack tip. This distribution can be obtained by solving the equation of motion for the order parameter discussed in the next section.

A. Equation of motion for a crack-transformational process zone complex

Within the scope of linear elastic fracture mechanics, steady crack propagation is described by the inertialess equation put forward by Freund [1]:

$$(1 - V/V_{\mathrm{R}})G = \Gamma, \tag{7}$$

where V is the crack speed; V_R is the Rayleigh velocity;

$$G = \frac{K_I^2(1-\sigma^2)}{E}; \quad \Gamma = \frac{K_{IC}^2(1-\sigma^2)}{E} \tag{8}$$

are the driving force and its threshold value; and K_I, K_{IC}, E, and σ are the stress intensity factor, the fracture toughness, Young's modulus, and Poisson's ratio. Equation (7) predicts that the crack velocity

$$V = V_R(1 - \Gamma/G) \tag{9}$$

increases monotonically from zero to V_R when the driving force increases from Γ to infinity [1]. Within the Freund approach, the terminal crack velocity, V_T (at $G \to \infty$), is, thus, equal to V_R.

The Freund's equation (7) disregards the contribution of the internal dynamics of the PZ to the crack motion. To take this into account, the friction force, $\Delta\Gamma$, (A5) should be added to the right-hand side of Freund's equation (7):

$$(1 - V/V_R)G = \Gamma + \Delta\Gamma. \tag{10}$$

III. PROCESS ZONE DYNAMICS

A. Equation of motion for the order parameter

Detailed derivation of the equation describing concerted zone-crack propagation is lengthy. It can be found in Ref. [58].

Here we only cite its key points. PZ dynamics is described by a system of equations

$$\kappa\frac{\partial\eta}{\partial t} = g\Delta\eta - [\alpha + 2A\varepsilon_{ii}(\mathbf{r})]\eta - \beta_0\eta^3,$$
$$\partial\sigma_{ik}/\partial x_k = 0, \tag{11}$$

where Δ is the Laplace operator; α depends on the temperature T as $\alpha = a(T - T_c)$, where $a > 0$ is a constant and T_c is the Curie temperature; and A is the so-called striction constant describing the interaction between the order parameter, η, and the elastic degrees of freedom. In general, it may have either sign. Further, $g > 0$ and $\beta_0 > 0$ are constants, and σ_{ik} is the stress tensor:

$$\sigma_{ik} = \frac{E\nu}{(1-2\sigma)(1+\sigma)}\varepsilon_{jj}\delta_{ik} + \frac{E}{1+\sigma}\varepsilon_{ik} + A\eta^2\delta_{ik}, \tag{12}$$

ε_{ik} is the strain describing both the contribution of the crack and that of the order parameter distribution, and δ_{ik} is the Kronecker symbol. The last term, $A\eta^2\delta_{ik}$, in (12) describes the spontaneous stress generated by the phase transition. For simplicity we omitted the inertial term in the second Eq. (11), which is valid if $V \ll c$, where c is the speed of sound.

Eliminating elastic degrees of freedom one comes to a single time-dependent Ginzburg-Landau equation,

$$\kappa\frac{\partial\eta}{\partial t} = g\Delta\eta - \left[\alpha + 2A\varepsilon_{ii}^{(0)}(\mathbf{r})\right]\eta - \beta\eta^3, \tag{13}$$

where the parameter β is expressed in terms of β_0 as follows:

$$\beta = \beta_0\left\{1 - \frac{2A^2}{E\beta_0}\frac{(1-2\sigma)(1+\sigma)}{1-\sigma}\right\} \tag{14}$$

and $\varepsilon_{ik}^{(0)}(r)$ is the strain field at the "undressed" (that is, $\eta = 0$) crack tip:

$$\varepsilon_{ii}^{(0)}(\mathbf{r}) = \frac{(1+\sigma)(1-2\sigma)K_I}{E(2\pi r)^{1/2}}\cos(\theta/2) \tag{15}$$

given by the the well-known elastic fracture mechanics expression [63]. Here r and φ are the polar coordinates centered at the crack tip and σ is the Poisson ratio. Let us note that Eqs. (13) and (15) account both for the elastic field of the crack as well as for that of the order parameter. Details on the derivation of Eq. (13) may be found in our paper [58].

Let us mention that far from the crack tip ($\varepsilon_{ii}^{(0)} \approx 0$) in equilibrium and at high temperatures ($\alpha > 0$) one finds the solid in the bulk phase $\eta = 0$, also referred to as the "mother phase," while at $T < T_c$ (corresponding to $\alpha \leqslant 0$), the bulk "daughter phase," $\eta = \pm(-\alpha/\beta)^{1/2}$, takes place, as should be expected from the theory of bulk phase transitions [18].

B. The automodel regime

Assuming that the crack tip propagates with velocity V along the Ox axis, and passing to the comoving frame, $x' = x - Vt$, $y' = y$, one obtains the configurational force:

$$\Delta\Gamma(V) = \kappa V\int\left(\frac{\partial\eta}{\partial x'}\right)^2 d^2r'. \tag{16}$$

Equation (13) together with (16) and (10) yields the system of equations:

$$g\Delta\eta + \kappa V\frac{\partial\eta}{\partial x'} - \left[\alpha \pm B\frac{\cos(\theta)}{\sqrt{r'}}\right]\eta - \beta\eta^3 = 0,$$
$$(1 - V/V_R)G = \Gamma + \kappa V\int\left(\frac{\partial\eta}{\partial x'}\right)^2 d^2r', \tag{17}$$

where

$$B = \frac{4|A|(1-2\sigma)(1+\sigma)}{\sqrt{2\pi}E}K_I > 0 \tag{18}$$

and one chooses the plus sign if $A > 0$ and otherwise the minus sign. Further, $r' = (x'^2 + y'^2)^{1/2}$, and the Laplace operator is defined as $\Delta = \partial^2/x'^2 + \partial^2/y'^2$. Since we only use the comoving frame, from here onward the primes are omitted.

Let us assume $\alpha > 0$ and describe the transformational PZ as a local daughter phase $\eta(\mathbf{r}) \neq 0$ embedded into the matrix of the bulk mother phase $\eta = 0$, localized at the crack tip, $(x, y) = 0$ and vanishing away from it. This is referred to as the "dressed crack tip." The boundary condition takes the form $\eta(\infty) = 0$, corresponding to no daughter phase away from the tip.

Equation (17) represents a closed system of equations with unknowns V and $\eta(\mathbf{r})$ describing the concerted, steady propagation of the crack and the process zone. We give its solution in the following section.

C. The propagating process zone

Let us consider the first equation, Eq. (17), regarding the velocity, V, as a parameter. It is nonlinear and exhibits a bifurcation. The full solution of the bifurcation problem is reported in our paper [58]. For the convenience of the reader, we below provide the results of Ref. [58] necessary for understanding our further arguments. For the sake of brevity, we only focus here on the case of a daughter PZ embedded in the matrix of the bulk mother phase.

At large values of α, (17) has the trivial solution $\eta = 0$. The bifurcation point, $\alpha = \alpha_* = a(T_* - T_c)$, has the form

$$\alpha_* = \frac{2^{2/3}}{\pi^{2/3}g^{1/3}}\left[\frac{|A|(1-2\sigma)(1+\sigma)}{E}\right]^{4/3} \times K_I^{4/3} - \frac{\kappa^2V^2}{4g}. \tag{19}$$

The LPT takes place at $\alpha < \alpha_*$, while at $\alpha > \alpha_*$ the crack tip is undressed. Since at $\alpha < 0$ the whole bulk of the solid transforms into the phase $\eta \neq 0$, the LPT domain is restricted to $0 < \alpha \leqslant \alpha_*$, where the solution of (17) takes the form [64]

$$\eta(\mathbf{r}) = \xi\Psi_*(\mathbf{r}), \tag{20}$$

where

$$\Psi_*(\mathbf{r}) = \exp\left[-\frac{V}{\sqrt[3]{4}V_*}\frac{r}{R}\cos(\theta) - \frac{r}{\sqrt[3]{4}R} + \sqrt[3]{4}\sqrt{\frac{r}{R}}\cos(\theta/2)\right] \tag{21}$$

defines the form of the order parameter distribution and the amplitude ξ has the form

$$\xi = \begin{cases} 0, & \alpha > \alpha_* \\ \pm\left(\frac{I_2}{I_4}\right)^{1/2}\left(\frac{\alpha_*-\alpha}{\beta}\right)^{1/2}, & \alpha \leqslant \alpha_*, \end{cases} \tag{22}$$

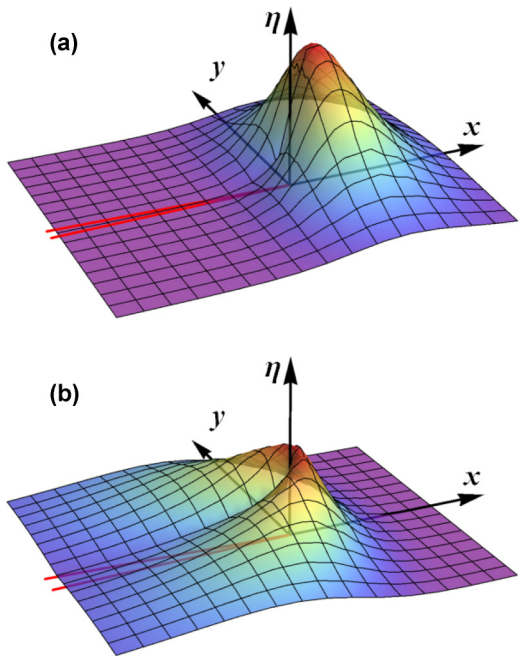

FIG. 1. The spatial distribution of the order parameter, $\eta(x,y)$, in the vicinity of a motionless (a) and a propagating (b) crack. Two red lines indicate the crack tip position.

The notations used in (21) and (22) are as follows:

$$V_* = \frac{2^{4/3} g^{1/3}}{\pi^{1/3}\kappa}\left[\frac{|A|(1-2\sigma)(1+\sigma)}{E}\right]^{2/3} K_I^{2/3}, \tag{23}$$

$$R = \left(\frac{g}{B}\right)^{2/3} = \frac{\pi^{1/3}}{2}\left[\frac{gE}{|A|K_1(1-2\sigma)(1+\sigma)}\right]^{2/3}, \tag{24}$$

while the factors I_n ($n = 2, 4$) are the integrals over the whole (x,y) plane:

$$I_n(V) = \int \Psi_*^n(\rho, V/V_*) d^2\rho, \tag{25}$$

depending on the crack velocity, V, and ρ is the dimensionless radius-vector: $\rho = r/R$.

The derivation of the solution (19)–(25) was explained and discussed in Ref. [58].

The solution (20), (22), and (21) is asymptotically exact [64]. The spatial distribution of the order parameter (20) is shown in Fig. 1. Here Fig. 1(a) displays the order parameter in the vicinity of the motionless crack tip, $V = 0$, while Fig. 1(b) demonstrates the case of a propagating crack. The image Fig. 1(b) was obtained at $V = 0.5V_*$.

D. Equation of the crack motion

The above results enable us to explicitly obtain the friction force (6) exerted on the crack tip. After the substitution of (20) into the second equation, Eq. (17), and integration, one derives the equation of the crack motion:

$$(1 - V/V_R)G = \Gamma + \begin{cases} 0, & \alpha > \alpha_* \\ \kappa V[\alpha_*(V) - \alpha]S(V)/\beta, & \alpha \leqslant \alpha_*, \end{cases} \tag{26}$$

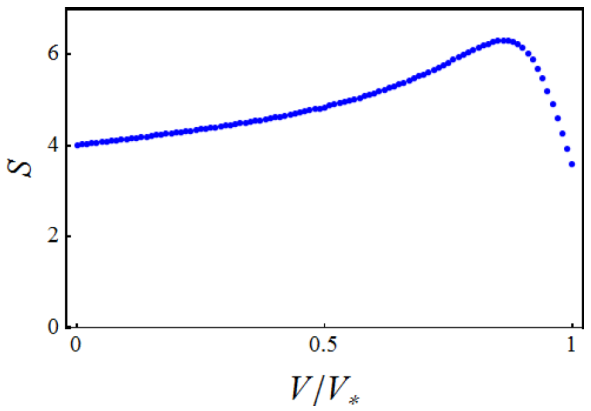

FIG. 2. Results of the numerical evaluation of the dependence of the combination of integrals (27) on the dimensionless velocity V/V_*.

where $S = S(V)$ is a dimensionless parameter depending on the crack velocity:

$$S(V) = \frac{I_2(V)}{I_4(V)} \int \left\{\frac{\partial \Psi_*(\mathbf{r}, V)}{\partial x}\right\}^2 d^2r. \tag{27}$$

For $V \neq 0$, the integrals (27) cannot be calculated analytically. Figure 2 shows the result of numerical evaluation of $S(V)$ by using the standard NIntegrate routine of MATHEMATICA 10, where we employed the even-odd subdivision method with a local adaptive strategy [65].

The nonlinearity of (26) manifests itself (i) in the nonlinear dependencies of $\alpha_*(V)$ (19) and $S(V)$ (27), as well as (ii) in its piecewise-smooth character. The nonlinearity gives rise to a bifurcation of its solution. A detailed, rather cumbersome, analysis of this equation can be found in Appendix A. Its results are presented in the next section.

IV. DYNAMICS OF A CRACK WITH THE TRANSFORMATIONAL PROCESS ZONE

A. Dimensionless parameters

Let us first introduce parameters α_c and V_c as

$$\alpha_c = \frac{2^{2/3}}{\pi^{2/3} g^{1/3}}\left[\frac{A(1-2\sigma)(1+\sigma)}{E}\right]^{4/3} K_{IC}^{4/3}, \tag{28}$$

$$V_c = \frac{2^{4/3} g^{1/3}}{\pi^{1/3}\kappa}\left[\frac{|A|(1-2\sigma)(1+\sigma)}{E}\right]^{2/3} K_{IC}^{2/3}. \tag{29}$$

In contrast to α_* and V_* (19) and (23), depending on the stress intensity factor, K_I, these parameters only depend upon material constants: g, A, E, σ, κ, and K_{IC}. Using (28) and (29) our results are most conveniently formulated in terms of dimensionless variables. Let us introduce

$$\tau_c = \alpha/\alpha_c \equiv (T - T_c)/[T_*(K_{IC}) - T_c] \tag{30}$$

defining the actual position on the phase diagram. At $T = T_c$ one finds $\tau_c = 0$, while $T = T_*(K_{IC})$ yields $\tau_c = 1$. Further, rather than the driving force, G, we will use the dimensionless parameter

$$\gamma = 1 - \Gamma/G, \tag{31}$$

referred to as the "*inverse driving force* " in the following. It is equal to zero when $G = \Gamma$ (that is, when the propagation starts) and turns into unity as soon as $G \to \infty$. Thus, the crack propagation takes place at $0 \leqslant \gamma \leqslant 1$.

The solution also depends on

$$v_c = V_c / V_R \tag{32}$$

defining the ratio of the critical and Rayleigh velocities and the dimensionless parameter:

$$k = \frac{\kappa V_R}{\beta \Gamma} \alpha_c v_c, \tag{33}$$

equal to the ratio of the amplitude of the viscouslike resistance force to Γ. It controls the effect of the PZ dynamics on the crack motion.

B. Characteristic plane

It is convenient to discuss regimes of cracks propagation in terms of the characteristic plane (γ, τ_c) representing the crack dynamics, with only the domain $\tau_c > 0$ and $0 \leqslant \gamma \leqslant 1$ being of importance. A point within this plane completely determines the crack motion, since γ defines the force driving the crack, while τ_c fixes the position of the solid at the phase diagram.

The crack velocity V depends on the inverse driving force, γ, Eq. (31), where $\gamma = 0$ at the left side of the characteristic plane corresponds to $V = 0$, while $\gamma = 1$ at its right side to the terminal velocity. Therefore, any crack propagation scenario maps onto a trajectory on the characteristic plane, referred to as the "crack evolution trajectory."

Below we only consider the simplest horizontal type of the trajectory. More complex ones are outside the scope of this paper.

C. Dynamics of the dressed crack

The characteristic plane is divided into two regions. In region I, no PZ at the crack tip takes place: the tip is "undressed." In region II the tip is "dressed," that is, a PZ is present. They are separated by the boundary:

$$\tau_c = \frac{1}{(1-\gamma)^{2/3}} - \left(\frac{\gamma}{v_c}\right)^2. \tag{34}$$

An analysis of the equation of crack motion (Appendix A) reveals three possible scenarios of the crack-PZ propagation.

The first of them takes place, if at $K_I = K_{IC}$ the temperature, T, exceeds $T_* = T_*(K_{IC})$ [Fig. 3(a)].

Let us denote by γ_0 the point where the crack evolution trajectory crosses the line (34) shown in Fig. 3(a). The crack tip is undressed while $\gamma < \gamma_0$. Correspondingly, the crack propagation is described by the solution (9) of the Freund equation (7). At the point $\gamma = \gamma_0$, the LPT zone emerges at the crack tip, giving rise to a configurational friction force. At $\gamma > \gamma_0$, the crack velocity exhibits a considerable decrease, followed by its further growth [Fig. 3(b)].

Figure 4(a) shows another scenario. Here the whole crack evolution trajectory lies within domain II, that is, the crack is always dressed. This gives rise to the solution which is all of non-Freund type and lies below the velocity corresponding to Freund's solution (9).

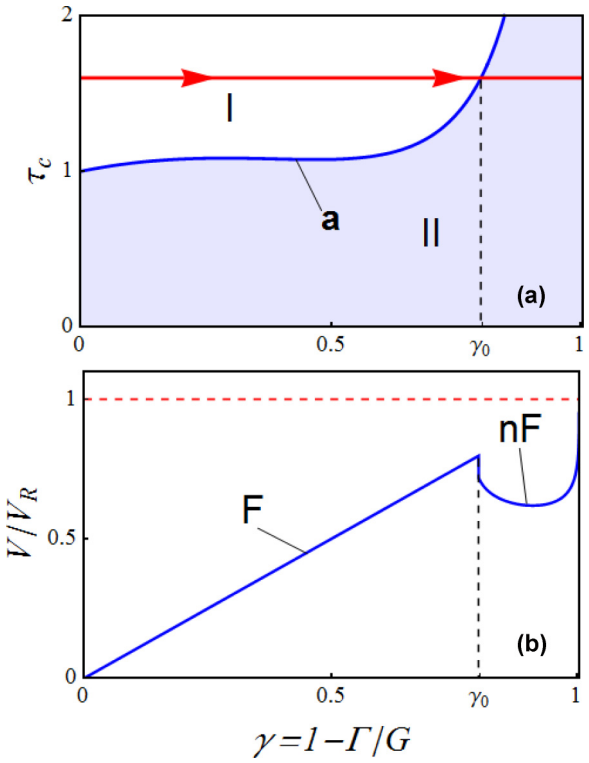

FIG. 3. The characteristic plane (a) and the corresponding dependence of the crack dimensionless velocity, V/V_R, on the inverse driving force, γ (a). The diagram has been obtained with $v_c = 0.7$ and $k = 0.3$. The characteristic plane (a) is separated into parts I and II. Within the latter the crack tip is dressed. The red arrow shows the position of the crack evolution trajectory. (b) The V/V_R dependence on γ corresponding to the crack evolution trajectory shown in panel (a). "F" indicates the part of the velocity with Freund's solution (9) while "nF" points out the one with the non-Freund solution described by Eq. (A11). The horizontal dashed line indicates the level of the Rayleigh velocity.

The scenarios shown in Figs. 3 and 4 always take place if the line of the boundary between regions I and II exhibits a monotonic growth.

In the case of nonmonotonic boundary behavior, one finds a third possible scenario, shown in Fig. 5(a). Let us consider a crack evolution trajectory starting from region II corresponding to the initially dressed crack. Its propagation obeys Eq. (26) and the speed is smaller than that predicted by Freund's solution (9). After it crosses the boundary

$$\tau_c \approx \frac{1}{(1-\gamma)^{2/3}} - 0.94\left(\frac{\gamma}{v_c}\right)^2 \tag{35}$$

at the point γ_{01}, the PZ vanishes and the undressed crack propagates with the velocity (9). One observes, therefore, a dramatic increase of the crack speed.

Under a further increase of the inverse driving force, the trajectory again enters the region II by crossing the line (34) at $\gamma = \gamma_{02}$. From this point onward, the crack tip is dressed, its motion obeying (26). That is, at this point, the velocity decreases. This gives rise to the $V = V(\gamma)$ dependence with

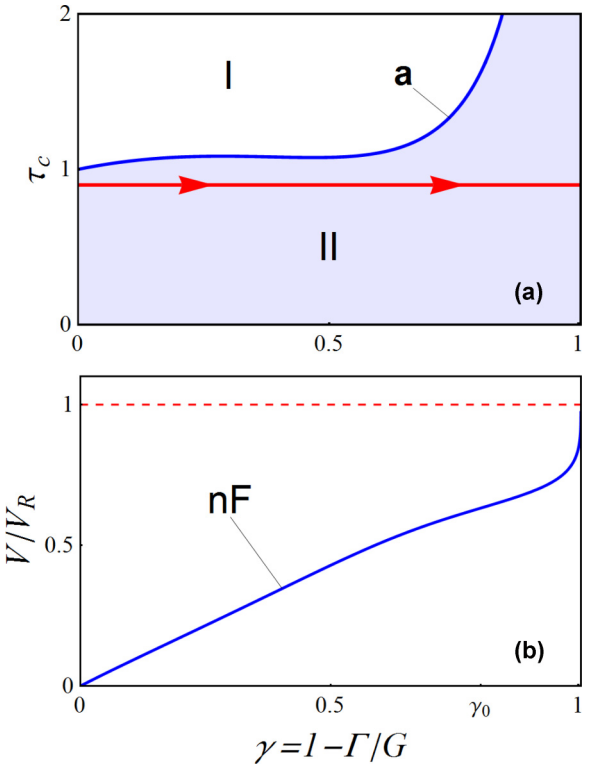

FIG. 4. The characteristic plane (a) is separated into parts without (I) and with the transformation zone at the crack tip (II). The red arrow shows the position of the crack evolution trajectory, which is in this case completely within domain II. (b) The V/V_R dependence on γ corresponding to the crack evolution trajectory shown in panel (a). In this case it is all of the non-Freund type. The horizontal dashed line indicates the level of the Rayleigh velocity. The diagram has been obtained with $\nu_c = 0.7$ and $k = 0.16$.

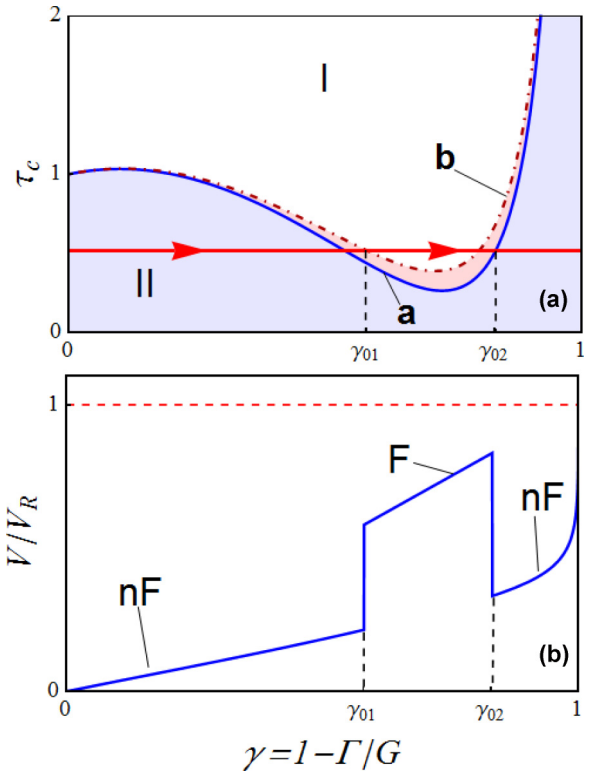

FIG. 5. (a) Characteristic plane with a nonmonotonic dependence of the boundary between regions I and II on the inverse driving force, γ. The crack evolution trajectory crosses the boundary between domains I and II twice. (b) The V/V_R dependence on γ corresponding to the crack evolution trajectory shown in panel (a). The diagram has been obtained with $\nu_c = 0.5$ and $k = 0.4$.

one Freund segment at $\gamma_{01} < \gamma < \gamma_{02}$ and two sections of the non-Freund type at $0 \leqslant \gamma \leqslant \gamma_{01}$ and $\gamma_{02} < \gamma < 1$. Note that due to the second-order nature of the LPT in the vicinity of the boundaries γ_{01} and γ_{02} the crack dresses or undresses gradually. Therefore, close to these points the velocity variation is continuous, although it may be rather steep.

The described scenario requires that both lines (34) and (35) exhibit a nonmonotonic behavior, which takes place at $\nu_c \lesssim 0.7$.

It should be mentioned that there is a fourth possible regime of the crack propagation. It can be realized if the starting point of the crack evolution trajectory is slightly above the point $\tau_c = 1$ but below the point of the maximum of the boundary between the regions I and II in Fig. 5(a). In this case the motionless crack is undressed, and it then dresses itself at a low speed and undresses again at a slightly higher speed. As in the previously described regimes the crack dresses again at a high velocity. This corresponds to the places where the crack evolution trajectory enters and then leaves region II in Fig. 5(a). The intervals of τ_c and ν_c at which this regime may exist are quite narrow, so this scenario can hardly be easily observed.

V. SIMULATIONS

A. Rescaling

The analytic solution obtained above is asymptotically exact. It is, however, only valid sufficiently close to the bifurcation point [64]. For this reason, away from this point we studied the problem numerically solving the system (17) by the finite-element method.

For this purpose, the system (17) has been first rescaled to make the variables dimensionless. This can be done by the replacement: $x \to d_1 x_1$, $y \to d_1 y_1$, and $\eta(x,y) \to d_2 u(x_1,y_1)$ with $d_1 = g/\kappa V_R$ and $d_2 = \kappa V_R/\sqrt{g\beta}$. The rescaled equations (17) take the form

$$\Delta_1 u + \frac{V}{V_R} \times \frac{\partial u}{\partial x_1} - \left[q_1 - \frac{\nu_c^{3/2}}{\sqrt{2(1-\gamma)}} \times \frac{\cos(\varphi/2)}{\sqrt{r_1}} \right] u - u^3 = 0,$$
$$\frac{V}{V_R} = \frac{\gamma}{1 + q_2(1-\gamma)\int \left(\frac{\partial u}{\partial x_1}\right)^2 dx_1 dy_1}, \tag{36}$$

where $\Delta_1 = \partial^2/\partial x_1^2 + \partial^2/\partial y_1^2$, $r_1 = (x_1^2 + y_1^2)^{1/2}$ and the control dimensionless parameters q_1 and q_2 are expressed as follows:

$$q_1 = \frac{\tau_c \nu_c^2}{4}; \quad q_2 = \frac{(\kappa V_R)^3}{g\beta\Gamma}.$$

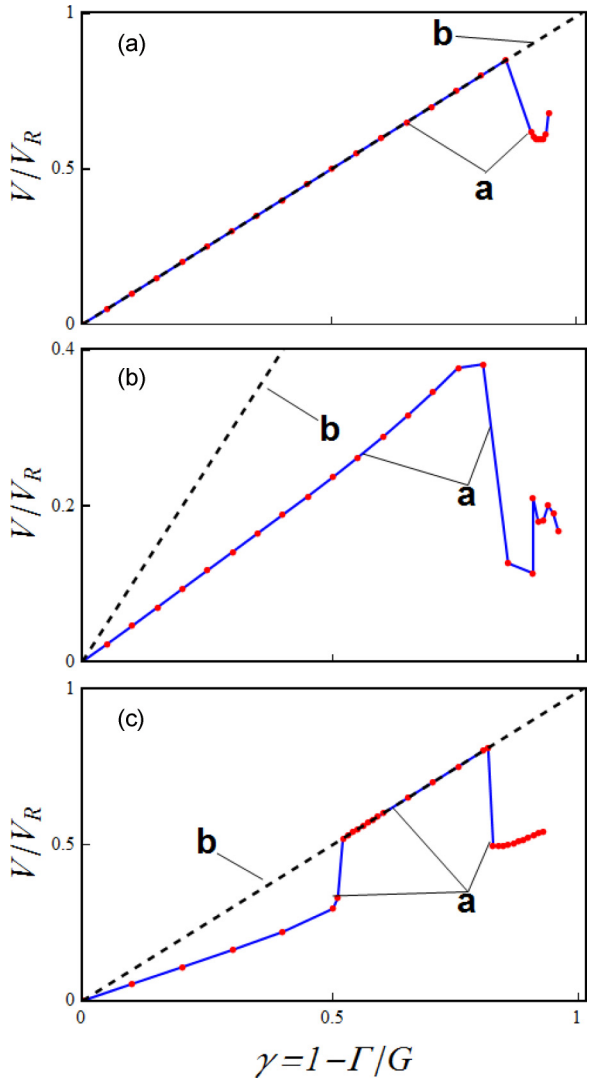

FIG. 6. Dimensionless crack velocity, V/V_R, dependent on the inverse driving force, $\gamma = 1 - \Gamma/G$ obtained by simulations. Dots show the simulation results, while the solid line (a) is drawn to guide the eye. The dashed line (b) shows Freund's solution $V/V_R = \gamma$. All the images were obtained with $\nu_c = 0.31$ and $q_2 = 0.9$. Panel (a) is obtained with $\tau_c = 1.9$, (b) with $\tau_c = 1.01$ and (c) with $\tau_c = 0.5$.

Technical details of our simulations are given in Appendix B, while their results are presented in the next section.

B. Results

The simulation results for $\nu_c = 0.31$ and $q_2 = 0.9$ are summarized in the image. Figure 6(a) has been obtained with $\tau_c = 1.9$. It corresponds to the crack evolution trajectory being almost entirely within the domain I, and only entering domain II at a high value $\gamma = \gamma_0 \approx 0.85$ (cf. Fig. 3). At $\gamma \leqslant \gamma_0$ the results coincide with the analytical solution $V/V_R = \gamma$, exhibiting the Freund behavior. At $\gamma > \gamma_0$ the solution is of the non-Freund type.

Figure 6(b), obtained at $\tau_c = 0.5$, shows the situation when the crack evolution trajectory lies entirely within the domain II, the crack tip being always dressed (cf. Fig. 4). In this case, the solution $V/V_R(\gamma)$ is everywhere of the non-Freund type. The numerical process converges poorly for γ close to unity. For this reason, we disregarded a few points in the close vicinity of $\gamma = 1$.

Figure 5(c) shows the case of a nonmonotonic I-II boundary. The solutions are of the non-Freund type at $\gamma < \gamma_{01}$, and $\gamma > \gamma_{02}$, while Freund's solution takes place at $\gamma_{01} < \gamma < \gamma_{02}$. In the simulated case, we obtained $\gamma_{01} \approx 0.52$ and $\gamma_{02} \approx 0.85$.

Figure 7 shows the distributions of the rescaled order parameter, $u = u(x_1, y_1)$, as a function of the dimensionless coordinates x_1 and y_1. All four images have been taken from the simulation with $\nu_c = 0.31$, $q_2 = 0.9$, and $\tau_c = 1.01$ reported in Fig. 6(c).

Figure 7(a) exhibits the case $\gamma = 0$ corresponding to a motionless crack, Fig. 7(b) shows the case $\gamma = 0.5$ which is a bit smaller, but close to γ_{01}, at which the velocity, V/V_R, exhibits an upward jump [Fig. 6(c)]. The order parameter distribution after the jump (at $\gamma = 0.52$) is displayed in Fig. 7(c). In this case, the height of the distribution is negligible and not visible within the scale of the image. We were only able to indicate it by an inhomogeneous color distribution. Finally, Fig. 7(d) demonstrates the order parameter right after the second jump (at $\gamma \geqslant \gamma_{02} \approx 0.85$).

Note that the distributions Figs. 7(b)–7(d) are stretched in the backward direction with respect to the distribution Fig. 7(a). This corresponds to our analytical predictions. On the other hand, the distributions Fig. 7 considerably differ from those displayed in Fig. 1 showing our analytic solution (21). This is since the analytic solution obtained within the branching theory is only valid in the vicinity of the bifurcation point. The latter is represented by the line separating the domains I and II in Figs. 3a, 4a, and 5(a). At a finite distance from this line, the solution obtained within the theory of branching yields a poor approximation.

VI. DISCUSSION

A. Results

We described the effect of the internal process zone dynamics on the steady crack propagation related to the dissipation following crystal lattice dynamic reconstruction. The corresponding force is viscous and nonlinear. The latter is due to the always-retarding reaction of the internal degree of freedom, the order parameter, on the crack motion. We argue that it gives rise to a non-Freund type of crack motion. In particular, we predict a regime in which increasing the driving force gives rise to an abrupt, jumplike variation of the crack velocity.

1. Observed cases of nonclassical crack motion

Discontinuities in the $V = V(G)$ dependence have been observed in silicon [4,5] and limestone [6]. In the former case simulations, indeed, show that the crack speed discontinuity is accompanied by the formation of a local clathrate phase [5], which is stable under a tensile stress [66], while experiments [67] suggest that local dynamic amorphization might also play a role in this phenomenon. Also, in the limestone case, one can point to a phase transition, presumably responsible for the speed jump [62]. In both materials the transitions behind the

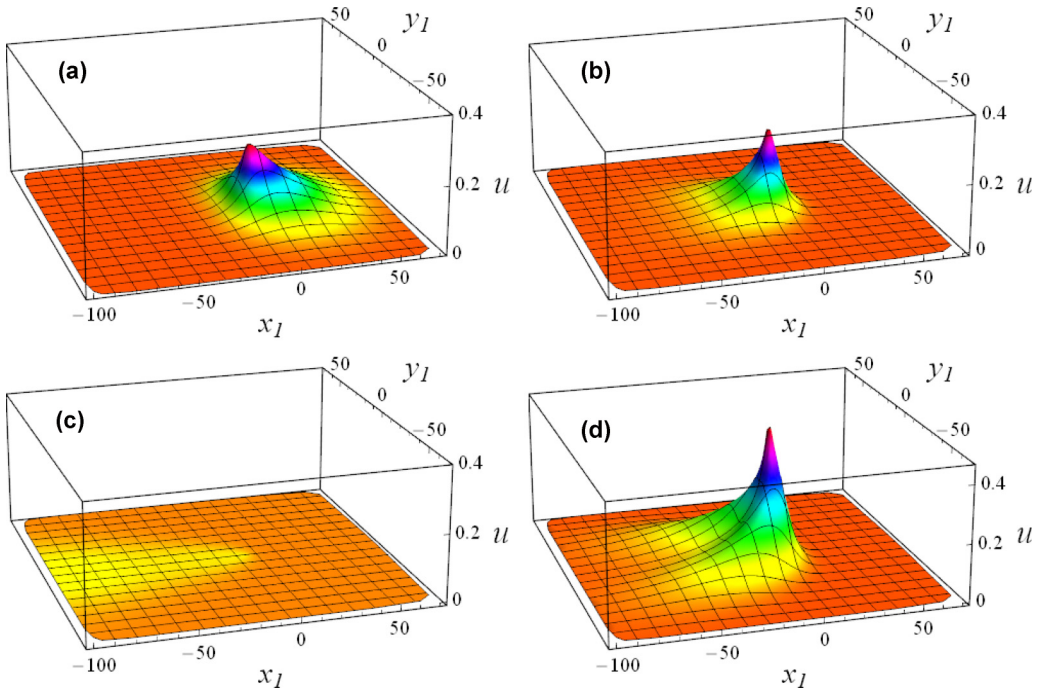

FIG. 7. The order parameter distrubution $u = u(x_1, y_1)$ obtained by our simulations with $\tau_c = 1.01$, $v_c = 0.31$, and $q_2 = 0.9$ (that is, for the case shown in Fig. 6(b). Panel (a) corresponds to the motionless crack, $\gamma = 0$, (b) to the case $\gamma = 0.5$ (before the first transition), (c) to $\gamma = 0.52$ (after the first transition), and (d) to $\gamma = 0.85$ (after the second transition).

velocity jumps are first-order ones, while here we only focused on the second-order LPTs.

2. *Limitations of the theory and conditions of its application*

With respect to the strain field, ε, the order parameters, η, are divided by the solid symmetry into two unequal classes with respect to the structure of the lowest-order invariant built on their combination: (i) the ones admitting a bilinear invariant ($\sim\varepsilon\eta$) in the solid free energy and (ii) those the lowest order invariant is linear-squared ($\sim\varepsilon\eta^2$). Note that the order parameter is often a multicomponent one.

The former case is restricted to the order parameters transforming as components of the tensors of the even rank under the action of the solid symmetry group, the order parameter equation containing the free term $\sim\varepsilon$. This case refers to the so-called proper ferroelastics, the materials for which the strain plays the role of the primary order parameter [68]. Pseudo-elastic nitinol represents the example of this case [69], as well as some other martensite-austenite transitions. This class of materials is out of the scope of the present theory.

The present theory applies to materials admitting the free-energy invariant $\sim\varepsilon\eta^2$ giving rise to the contribution $\sim\eta\varepsilon$ into the order parameter equation (11), where η represents the primary, while ε is the secondary order parameter. The latter class lacks the symmetry limitations of the ferroelastics and, therefore, is much more numerous. From a theoretical point of view, however, its description is more simple.

We described the nonlinear, viscous friction force acting on the crack tip using the simplest-possible model assuming a purely dilatant transformation, cf. the term $\eta\varepsilon_{ii}$ in Eq. (11) and a one-component order parameter. Its simplicity serves to reveal physical mechanisms behind the velocity jumps phenomenon. Accounting for the nondeviatoric terms is simple, but cumbersome, while accounting for the multicomponet η character is straightforward, but it is only reasonable to focus on for the description of a specific material.

3. *Second-order LPT versus the first-order one*

Crack tip dynamics affected by a first-order LPT has been briefly addressed in our recent publication [62] and will be considered in detail in a forthcoming paper. Being very complex, the description of the dynamics of the first-order transition is based on some additional assumptions that are not always satisfactorily justified. Therefore, the cases admitting a rigorous mathematical treatment are of paramount importance, providing such justifications and offering new insights. We focused here on the second-order LPTs motivated by the fact that since it is continuous, bifurcation theory techniques can be applied [62], enabling us to obtain rigorous analytical results at least in the vicinity of the bifurcation point. Our simulations lend this additional support. They together represent a basis on which a more complex first-order LPT dynamics [62] is grounded.

The above results are, however, not only important for theoretical reasons. Indeed, many transitions in nature are of the second order or of the so-called first order close to the second [70]. In the latter case they can be treated in a very similar way [71,72] and the most important results of the present analysis apply directly.

4. *Where the local phase transition takes place*

We relate the LPT to the phase diagram in the coordinates (T, p), where p is the hydrostatic pressure. We have shown that LPT depends on the actual phase diagram position of the

solid (typically fixed by $p = 0$ and the temperature, T) with respect to the phase transition line, $T_c = T_c(p)$. We predict that the LPT at the crack tip can only take place on one side of the phase transition line determined by the sign of the striction constant A. The latter is directly related to the slope of the transition line, dT_c/dp. If $dT_c/dp > 0$, then the LPT only takes place below the transition line, while it is above the transition line for $dT_c/dp < 0$ [58,62]. For the sake of brevity, in this paper we only presented the calculations for the latter case. All the results, however, apply also to the former case, up to numeric factors.

5. Regimes of concerted crack-zone propagation

We, further, predict four regimes of crack propagation.

The first regime takes place if the actual solid position in the phase diagram is far from the phase transition line, and the motionless crack exhibits no transformational PZ. In this case the zone only emerges at a high crack speed. At smaller speeds the propagation is described by the classical Freund law (9) and only exhibits nonclassical behavior after the zone shows up. It should be mentioned that in practice this may take place at a crack speed difficult to access experimentally.

The second regime occurs if the actual state is below the transition line in the phase diagram. Then the LPT exists for a motionless as well as for a propagating crack. In this case, the crack propagation is everywhere of a non-Freund type.

If the actual state is below the phase transition line (as in the latter case), but the line of the phase transition in the plane (γ, τ_c) is nonmonotonic, then a flickering behavior takes place, which is the third regime. The transformation zone already exists at the tip of the motionless crack and persists unless the crack speed exceeds a certain value. Then it vanishes to reappear once more at a high velocity.

The zone's vanishing and emergence taking place within the first and the third scenarios are accompanied by an alteration of the motion regime. This takes place in a jumplike way in the case of a first-order phase transition but continuously in the second-order case. The latter continuous change is, however, rather abrupt, looking pretty much like jumps in our simulations. It is this regime that presumably takes place during the dynamic fracture of silicon and limestone [4–6].

A fourth regime is also possible, in which no zone exists at the motionless tip but emerges at a small crack speed, and again disappears at a larger one and finally reappears at a high speed. This regime, however, is only possible within a narrow temperature interval.

B. Effect of the zone on the crack motion

To show a noticeable experimental effect, the two following conditions should be fulfilled.

1. Region of the zone's existence

First, the LPT phenomenon should take place in a wide-enough part of the phase diagram. Here we briefly recite the results of this phase diagram analysis discussed in details in our papers [58,62].

The absolute value of $\Delta T_* = T_* - T_c$ depends on the striction constant, A (related to the slope of the phase transition). The latter can have any value and sign. One observes, however, that the transition line slope exhibits a typical order of magnitude: $dT_c/dp \sim 1$ to 10 K / kbar [70]. Combined with other typical parameters of solids entering the result (19) one finds that the typical value of ΔT_* is from $\sim$100 to $\sim$1000 K [58,62]. Taking into account that the melting temperature of solids typically falls in this same interval, one concludes that the region of existence of the transformational PZ covers a considerable part of the phase diagram or even the whole phase diagram on one side of the corresponding phase transition line [58,62]. From these estimates for the typical values of ΔT_*, one concludes that the transformational PZ should be expected in a wide part of the solid phase diagram.

We did not find papers reporting a transformation PZ and ΔT_* values for materials exhibiting a second-order local phase transition. It should be noted, however, that the estimates for ΔT_* given above are valid not only for second-order transitions [58] but also for the first-order ones, as shown in Ref. [62]. For this reason, below we point out several materials exhibiting first-order local phase transformations for which such information is available.

It should be mentioned that the width $\Delta T_* \approx 300$ K of the region of existence of the transformational PZ has been, indeed, observed during the glass transition at the tip of a propagating crack in NiTi [73]. Other papers have not revealed the whole region of existence. Some of them, however, report an observation of an LPT at a considerable "distance" from the bulk phase transition: over 200 K in Ni-Al [74].

The width ($\sim$100 to $\sim$1000 K) of the phase diagram region of the LPT existence considerably exceeds the typical width ($\sim$1 to $\sim$10 K) of the hysteresis zone [70]. One concludes that in most cases LPTs should be expected outside of the hysteresis. This, however, implies that the zone only emerges when the crack is loaded and vanishes upon unloading, making it difficult to be detected.

2. Quantitative estimate of the zone effect

Second, let us see how strong the PZ impact is. This can be quantified by estimating the ratio between the jump of the crack velocity and the Rayleigh speed. Making use of the expressions (10), one can define the difference, ΔV, between the velocity of the dressed and undressed cracks as $\Delta V/V_R = \kappa\eta^2 V/G$. To make numerical estimates, let us define its value at $G = 2\Gamma$ and $V = V_R/2$, quantifying the PZ intensity:

$$\Delta V/V_R \sim \frac{\kappa\eta^2 V_R E}{4K_{IC}^2}. \tag{37}$$

We only address here second-order phase transitions. It is a common opinion that the effect of the second-order transition is small, since it is always proportional to η^m with $m > 0$. This is, however, only true in the close vicinity of the PT or bifurcation point, where η is small. Upon its emerging, the order parameter rapidly increases, achieving its saturation in about 10 to 100 K. Since it is matched or even exceeds by ΔT_*, one concludes that it is the saturated η value that typically enters (37).

In ferroelectrics the saturated order parameter value may be estimated in terms of the elementary charge, e, and the crystal lattice parameter, b, as $\eta \sim e/b^2$. Assuming $e = 4.8 \times 10^{-10}$ CGSE, $b \sim 1$ nm, $V_R \sim 10^5$ cm / s, $E \sim 10^{12}$ erg cm^{-3}, and $K_{IC} \sim 10^8$ erg cm$^{-5/2}$ typical for inorganic solids one finds that at $\kappa \gtrsim 10^{-9}$ s the intensity $\Delta V / V_R \gtrsim 0.1$.

The kinetic factor κ can take the value of $\kappa \sim 10^{-7}$ s as in the case of $AgNa(NO_2)_2$, $\kappa \sim 10^{-11}$ s as in KNO_3 or $NaNO_2$, $\kappa \sim 10^{-12}$ s as in the Rochelle Salt, triglycine sulfate, and KD_2PO_4 down to $\kappa \sim 10^{-13}$ s as in $BaTiO_3$, $PbTiO_3$, $Pb(Ti_x,Zi_{1-x})O_3$, and $SrTiO_3$ [21].

One concludes that in the case of order-disorder transitions with $\kappa \gtrsim 10^{-9}$ s the effect of the LPT on the crack tip dynamics is strong. The crack velocity discontinuity taking place within the scenario shown in Fig. 5 in such cases is considerable.

One should, further, keep in mind that most of the inorganic solids exhibit several phase transitions, some of them at low and others at high temperatures. One concludes that the crack tip PZ may be expected to contain several, rather than a single phase. In such a case, both phases will contribute to the friction force $\Delta\Gamma$, enhancing the zone effect. Indeed, two PZ phases, an amorphous and a martensite one, have been detected as coexisting at the tip of a propagating crack in NiTi [75].

VII. SUMMARY

To summarize, we present the dynamics of a transformational process zone at the tip of a steadily propagating crack. We derived a viscouslike configurational force exerted on the tip and resisting the motion of the crack. Its origin is due to the energy dissipation in the course of the evolution of the internal degrees of freedom responsible for the local phase transition. This enabled us to include into Freund's equation of crack propagation a component taking into account the transformational process zone. By solving this equation together with the one describing the order parameter dynamics, we predicted the region in the phase diagram in which the zone exists, as well as three regimes of crack propagation, depending on the actual position of the solid in the phase diagram. The first of them takes place if the solid is outside the zone existence region. In this case, the crack tip is undressed up to very high values of the driving force, which are hardly accessible experimentally. The crack exhibits here the dynamics predicted by Freund's equation. The second regime corresponds to the solid always staying within the region of the zone existence. In this case, the zone is always present, and the crack behavior considerably deviates from the predictions of linear elasticity fracture mechanics. In the third regime the solid leaves and enters the region of the zone existence. In this case the crack motion changes its character between the Freund and non-Freund types, exhibiting jumps during the transitions between them.

ACKNOWLEDGMENTS

One of us (A.L.K.) was supported by the DFG (Germany), Grant No. BA 944/4-1 and RFBR (Russia) Grant No. 13-02-91332.

APPENDIX A: ANALYSIS OF THE EQUATION OF MOTION

1. Concise form of the equation of motion

The equation of motion has the most concise form admitting analysis if one writes it down in terms of the dimensionless parameters

$$\tau = \alpha/\alpha_* \equiv (T - T_c)/(T_* - T_c), \tag{A1}$$

$$\nu = V_*/V_R, \tag{A2}$$

and the dimensionless velocity

$$\omega = V/V_*. \tag{A3}$$

These parameters differ from the ones already introduced above [(30) and (32)] since they depend on K_I rather than on its threshold value K_{IC}.

For later use, let us list the relations among the K_I-dependent parameters ω (A3), ν (32), and τ (A1) and the K_{IC}-dependent ones v_c and τ_c:

$$\tau = \tau_c(1-\gamma)^{2/3}; \quad \nu = \frac{v_c}{(1-\gamma)^{1/3}}; \quad \omega = \frac{V}{V_R}\frac{(1-\gamma)^{1/3}}{v_c}. \tag{A4}$$

In terms of ω and τ the configurational force $\Delta\Gamma$ can be rewritten in the following form:

$$\Delta\Gamma = \kappa V_c \frac{\alpha_c}{\beta}\begin{cases} J(\omega,\tau), & 1-\omega^2-\tau > 0 \\ 0 & 1-\omega^2-\tau \leqslant 0 \end{cases}, \tag{A5}$$

where the dimensionless function J has the form:

$$J(\omega,\tau) = \omega(1-\omega^2-\tau)S(\omega). \tag{A6}$$

The integral expression $S = S(\omega)$ (27) has been evaluated numerically. Using the FindFit routine of MATHEMATICA [65], the function $J(\omega,\tau)$ has been further fitted to the following polynomial:

$$J(\omega,\tau) \approx c_1\omega - c_3\omega^3 \tag{A7}$$

with

$$c_1 \approx 4.85 - 5.57\tau + 0.73\tau^2; \quad c_3 \approx 4.49 - 0.36\tau. \tag{A8}$$

The numerical results along with the fitting are shown in Fig. 8.

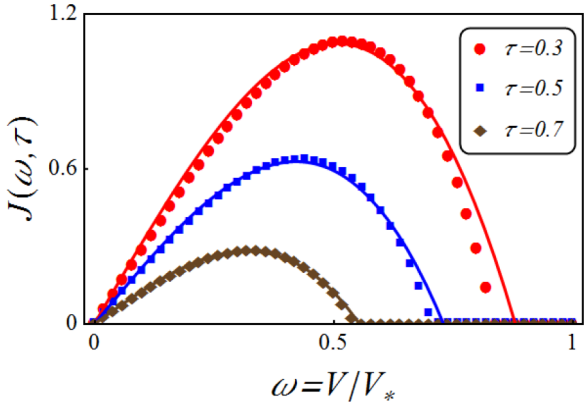

FIG. 8. The function J obtained by the numerical integration (points) and its fitting by Eq. (A7) (solid lines).

The function $J(\omega,\tau)$ exhibits a nonlinear dependence on the dimensionless velocity ω as shown in Fig. 8. At a small crack velocity, ω, one finds $\Delta\Gamma \sim \omega$, that is, the configurational resistance force behaves as a viscous friction force. At high velocities, however, $\Delta\Gamma$ dramatically changes its behavior. In particular, as soon as the velocity achieves a value at which the order parameter η vanishes, the PZ disappears and the friction force becomes zero.

In terms of the K_I-dependent parameters ω, k (33), ν, and τ equation of the crack motion can be written in the simple form

$$\gamma - \omega \times \nu = k\omega \times \begin{cases} c_1 - c_3\omega^2, & 1-\omega^2-\tau > 0 \\ 0, & 1-\omega^2-\tau \leqslant 0 \end{cases}. \quad \text{(A9)}$$

This is a nonlinear, piecewise smooth equation describing steady crack propagation. Its solution yields the dimensionless velocity, ω, of the joint crack-PZ propagation. A detailed analysis of this equation is in the next section.

2. Analytical approach

For $1-\omega^2-\tau < 0$, the equation of motion (A9) is linear, with the solution $\omega = \gamma/\nu$ yielding

$$V/V_R = \gamma, \quad \text{(A10)}$$

which is equivalent to the solution (9) of Freund's equation (7).

In the opposite case, $1-\omega^2-\tau > 0$, (A9) is a cubic equation. Among its three solutions we are looking for a positive one, approaching zero as $\gamma \to 0$. This behavior is only exhibited by the solution

$$\omega = \frac{(i\sqrt{3}-1)(kc_1+\nu)}{2^{2/3}Q} - \frac{(1+i\sqrt{3})Q}{6\times 2^{1/3}kc_3} \quad \text{(A11)}$$

with $Q=\{3kc_3[81\gamma^2c_3^2k^2-12kc_3(kc_1-\nu)^3]^{1/2}-27\gamma c_3^2k^2\}^{1/3}$. Here $c_{1,3}=c_{1,3}(\tau)$ are given by (A8). Though expressed in terms of complex numbers, it is not difficult to see that the solution (A11) is real.

The PZ emerges or disappears as soon as $\tau = \tau_*$ holds, where τ_* obeys the equation:

$$1-\omega^2-\tau_* = 0, \quad \text{(A12)}$$

provided ω is one of the solutions (A10) or (A11) of the equation of motion (A9).

a. Dressing condition

If the crack is initially undressed, then the equation defining the line in the characteristic plane on which the PZ emerges is obtained by substituting the "undressed" solution $\omega = \gamma/\nu$ into (A12), yielding $\tau_* = 1-(\gamma/\nu)^2$ for the equation of emergence line (34).

b. The undressing condition

If the speed of the initially dressed crack is increased, then the transition to the undressed state takes place already at $\tau < 1-(\gamma/\nu)^2$.

Figure 9 shows the graphical solution of the equation of motion (A9), the right-hand part of it being indicated by (a). A few positions of the left-hand part, corresponding to different γ, are shown by the straight lines (b), (c), and (d). We analyze the case with an initially dressed crack starting from $\gamma = 0$, followed by its gradual increase. In the position shown by (b) (A9) has a single solution (shown by a dot). It is the nonlinear solution (A11) of the cubic equation (A9) corresponding to the dressed crack.

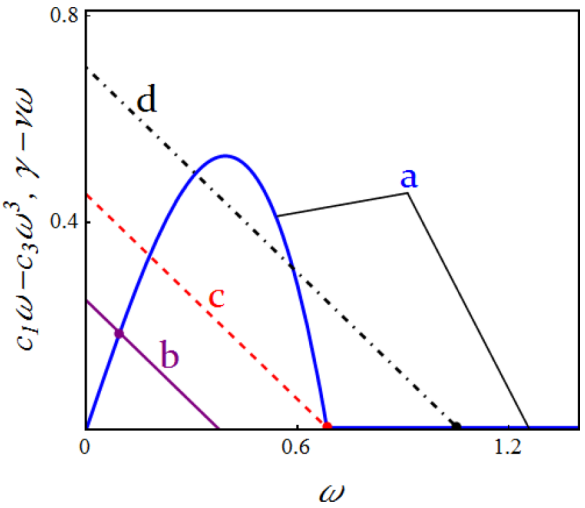

FIG. 9. Graphical solution of the equation of motion (A9). Line (a) shows the piecewise smooth right-hand side of the equation of motion: $c_1\omega - c_3\omega^3$ for $1-\omega^2-\tau < 0$ and 0 in the opposite case. Lines (b), (c), and (d) show the left-hand side of the equation of motion for different γ. Dots indicate the solution actually taking place. The case of an initially dressed crack corresponds to γ increasing from zero. For small γ one finds a single point of intersection of the lines (a) and (b) corresponding to the non-Freund solution. Line (c) corresponds to the transition from the non-Freund to the Freund solution at the intersection of line (c) with the abscissa. For larger γ, shown by line (d), of the three possible solutions of (A9), only the one lying on the abscissa takes place.

As soon as γ increases in such a way that the corresponding line takes the position (c), the second solution emerges, while for the position (d) one finds three solutions. Two of them are the solutions of the cubic equation, while the third is the one given by Eq. (A10). It corresponds to an undressed crack.

In the situation with several solutions, one needs a criterion with which to choose, which one takes place. We here use the following criterion: the solution that survives must correspond to the smallest resistance for the crack propagation. According to this criterion, one concludes that for both (c) and (d) the surviving solution is (A10). Therefore, the transition from the dressed to the undressed state takes place under the conditions corresponding to the parameters indicated by (c) in Fig. 9.

Let us now find the condition controlling this bifurcation. The surviving solution satisfies both $\gamma - \omega\nu = 0$ and $c_1(\tau) - c_3(\tau)\omega^2 = 0$ [(c) in Fig. 9] yielding $\gamma = \nu[c_1(\tau)/c_3(\tau)]^{1/2}$. The latter represents the equation for the undressing line. One observes that the function $[c_1(\tau)/c_3(\tau)]^{1/2}$ can be very accurately approximated by the expression $1.034(1-\tau)^{1/2}$, as shown in Fig. 10.

Passing now to the K_{IC}-dependent coordinates with (A4), one finds the undressing condition (35).

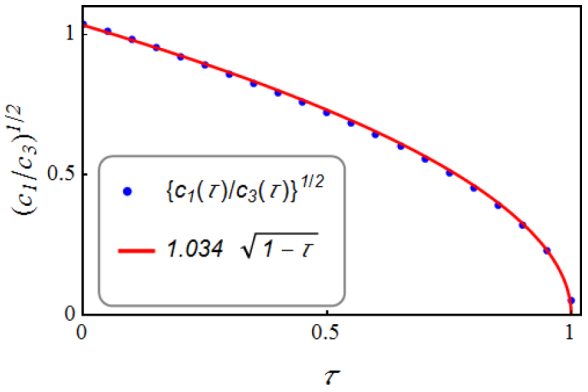

FIG. 10. Approximation of $[c_1(\tau)/c_3(\tau)]^{1/2}$ (dots) by $1.034(1-\tau)^{1/2}$ (solid line).

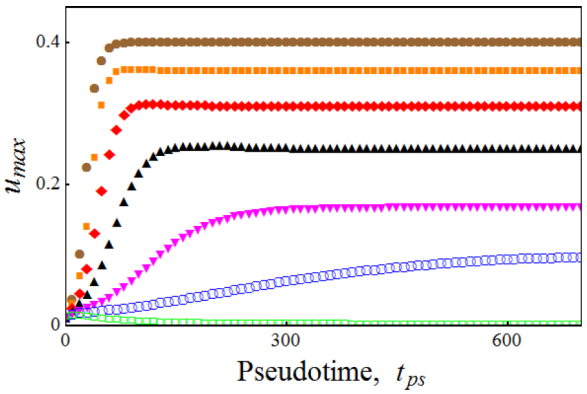

FIG. 11. The illustration of the convergence of the calculations with the pseudotime. It shows the dependence of the amplitude, $u_{\max}$, of the dimensionless order parameter, u, on the pseudotime for different q_1 values. Filled diamonds: $q_1 = 0.3$; empty diamonds: 0.32; filled squares: 0.34; filled hexagons: 0.36; up-triangles: 0.38; down-triangles: 0.39; empty squares: 0.41. Note that in the case of $q_1 = 0.39$ (down-triangles) the $u_{\max}(t)$ dependence still exhibits a slope and for satisfactory convergence, a longer process was used (not shown).

APPENDIX B: SIMULATIONS, THE TECHNICAL DETAILS

We used the software COMSOL 4B for the simulations. The equations have been simulated in the half-plane $y \geqslant 0$. A semielliptic domain has been defined by trial and error, such that the solution vanishes well before the domain boundaries. The no-flux boundary condition has been set at the boundary $y = 0$ and the Dirichlet condition $u = 0$ at the rest of its boundary. A straightforward simulation of the static equation (36) with such boundary conditions, however, only returns the trivial solution.

To avoid this we introduced a pseudodynamic equation:

$$\frac{\partial u}{\partial t_{\rm ps}} = \Delta u + \frac{V}{V_R}\frac{\partial u}{\partial x} - \left[q_1 - \frac{v_c^{3/2}}{\sqrt{2(1-\gamma)}}\frac{\cos(\varphi)}{\sqrt{r}}\right]u - u^3 \tag{B1}$$

instead of the first equation (36). Here $t_{\rm ps}$ is the pseudotime. A stable solution of the static equation (36) represents a fixed point of the dynamic one. As the initial condition, we used a smoothed step function, only differing from zero in some vicinity of the point (0,0). The integral equation has been defined using the Model Coupling option of COMSOL.

The dynamic system has been solved using the direct MUMPS solver with BDF time stepping. The convergence of the solution to its fixed point has been controlled by the behavior of the $u_{\max}$, the maximum value of the function $u(x,y)$. By trials we found that 700 pseudotime steps ensure a good convergence, though sometimes it has been necessary to bring the process up to 3000 steps. Figure 11 shows an example of such a convergence study for a number of simulations in which all parameters except q_1 were fixed, while q_1 was varied.

One can see that, far from the bifurcation point, convergence takes place well before 700 pseudotime steps are done. As can be expected, the situation differs close to the bifurcation ($q_1 = 0.38$ and 0.39 corresponding to up-triangles and down-triangles in Fig. 11). Even here, 700 pseudotime steps guarantee a rather reliable convergence.

[1] L. B. Freund, *Dynamic Fracture Mechanics* (Cambridge University Press, Cambridge, 1998).
[2] J. Fineberg and M. Marder, Phys. Rep. **313**, 1 (1999).
[3] J. E. Field, Contemp. Phys. **12**, 1 (1971).
[4] J. A. Hauch, D. Holland, M. P. Marder, and H. L. Swinney, Phys. Rev. Lett. **82**, 3823 (1999).
[5] M. J. Buehler, H. Tang, A. C. T. van Duin, and W. A. Goddard, Phys. Rev. Lett. **99**, 165502 (2007).
[6] A. Bertram and J. F. Kalthoff, Key Eng. Mater. **251-252**, 423 (2003).
[7] S. J. Pennycook, Ultramicroscopy **123**, 28 (2012).
[8] S. J. Wang, H. Wang, K. Du, W. Zhang, M. L. Sui, and S. X. Mao, Nat. Commun. **5**, 3433 (2014).
[9] S. W. Robertson *et al.*, Acta Mater. **55**, 6198 (2007).
[10] I. Roth *et al.*, in *ESOMAT 2009-8th European Symposium on Martensitic Transformations*, edited by P. Sittner, V. Paidar, and H. Seiner (EDP Sciences, Ulis, France, 2009).
[11] S. Daly *et al.*, Acta Mater. **55**, 6322 (2007).
[12] X. Tan *et al.*, Acta Mater. **62**, 114 (2014).
[13] F. Meschke *et al.*, J. Am. Ceram. Soc. **83**, 353 (2000).
[14] Y. H. Lu *et al.*, Intermetallics **10**, 823 (2002).
[15] E. Sgambittera, C. Maletta, and F. Furgiuele, Sripta Matter **101**, 64 (2015).
[16] E. Bouchbinder, A. Livne, and J. Fineberg, Phys. Rev. Lett. **101**, 264302 (2008).
[17] H. Gao, J. Mech. Phys. Solids **44**, 1453 (1996); M. J. Buehler and H. Gao, Nature **439**, 307 (2006).
[18] L. D. Landau and E. M. Lifshitz, *Statistical Physics* (Pergamon Press, Oxford, 1985), Secs. 120 and 121.
[19] A. Karma, D. A. Kessler, and H. Levine, Phys. Rev. Lett. **87**, 045501 (2001); V. Hakim and A. Karma, *ibid.* **95**, 235501 (2005); R. Spatschek, M. Hartmann, E. Brener, and H. Müller-Krumbhaar, *ibid.* **96**, 015502 (2006).
[20] M. C. Cross and P. C. Hohenberg, Rev. Mod. Phys. **65**, 851 (1993).

[21] A. D. Bruce and R. A. Cowley, *Structural Phase Transitions* (Taylor & Francis, London, 1981); M. L. Lines and A. M. Glass, *Principles and Applications of Ferroelectrics and Related Materials* (Oxford University Press, Oxford, 2001).

[22] P. Toledano and V. Dmitriev, *Reconstructive Phase Transitions*, in *Crystals and Quasicrystals* (World Scientific, Singapore, 1996).

[23] V. P. Dmitriev, S. B. Rochal, Y. M. Gufan, and P. Toledano, Phys. Rev. Lett. **60**, 1958 (1988); **62**, 844 (1989).

[24] S. R. Shenoy, T. Lookman, A. Saxena, and A. R. Bishop, Phys. Rev. B **60**, R12537 (1999).

[25] S. O. Kramarov, N. Y. Egorov, and L. M. Katsnel'son, Sov. Phys. -Solid State **28**, 1602 (1986); A. A. Grekov, Y. V. Dashko, S. O. Kramarov *et al.*, Ferroelectrics Lett. **8**, 59 (1988); C. S. Lynch, R. M. McMeeking, and Z. Suo, in *Second International Conference on Intelligent Materials, ICIM '94*, edited by C. A. Rogers and G. G. Wallace (Technomic Publishing, Lancaster, PA, 1994), p. 856.

[26] G. G. Siu and W. G. Zeng, J. Mater. Sci. **28**, 5875 (1993).

[27] M. Kerr, M. R. Daymond, R. A. Holt *et al.*, Scr. Matter **62**, 341 (2010).

[28] T. Sasaki *et al.*, J. Ceram. Soc. Japan **120**, 473 (2012).

[29] J. Karger-Kocsis and J. Varga, J. Appl. Pol. Sci. **62**, 291 (1996); J. Karger-Kocsis, J. Varga, and G. W. Ehrenstein, *ibid.* **64**, 2057 (1997); H.-J. Sue, J. D. Earls, and R. E. Hefner, Jr., J. Mater. Sci. **32**, 4039 (1997); S. T. Kim *et al.*, *ibid.* **33**, 2421 (1998); G. A. Maier *et al.*, Macromolecules **38**, 6099 (2005); T. Koyama, T. Araki, and H. Tanaka, Phys. Rev. Lett. **102**, 065701 (2009).

[30] J. A. Horton, J. L. Wright, and J. H. Schneibel, in *Bulk Metallic Glasses*, edited by W. L. Johnson, A. Inoue, and C. T. Liu (Cambridge University Press, Cambridge, UK, 1999), Vol. 554, p. 185.

[31] J. A. Donovan, Nippon Gomu Kyokaishi **75**, 239 (2002); S. Trabelsi, P.-A. Albouy, and J. Rault, Macromolecules **35**, 10054 (2002); H. P. Zhang, J. Niemczura, G. Dennis, K. Ravi-Chandar, and M. Marder, Phys. Rev. Lett. **102**, 245503 (2009); J.-B. Le Cam and E. Toussaint, Macromolecules **43**, 4708 (2010); N. Saintier, G. Cailletaud, and R. Piques, Mater. Sci. Eng. **A528**, 1078 (2011).

[32] K. Nishimura and N. Miyazaki, CMES: Comp. Model. Eng. Sci. **2**, 143 (2001).

[33] Y.-F. Guo and D.-L. Zhao, Mater. Sci. Eng. **A448**, 281 (2007); Y.-F. Guo, Y.-S. Wang, and D.-L. Zhao, Acta Mater. **55**, 401 (2007).

[34] A. Latapie and D. Farkas, Modell. Simul. Mater. Sci. Eng. **11**, 745 (2003); R. Matsumoto *et al.*, CMES: Comp. Model. Eng. Sci. **9**, 75 (2005); I. R. Vatne *et al.*, Mater. Sci. Eng. **A560**, 306 (2013).

[35] D. Sherman, M. Markovitz, and O. Barkai, J. Mech. Phys. Solids **56**, 376 (2008); F. Atrash and D. Sherman, *ibid.* **60**, 844 (2012).

[36] J. R. Kermode *et al.*, Nature **455**, 1224 (2008).

[37] J. Mei *et al.*, Int. J. Solids Struct. **48**, 3054 (2011).

[38] M. Ruda, D. Farkas, and G. Bertolino, Comp. Mater. Sci. **49**, 743 (2010).

[39] Y. Zhang *et al.*, J. Nucl. Mater. **430**, 96 (2012).

[40] A. Falvo *et al.*, J. Mater. Eng. Perform. **18**, 679 (2009).

[41] B. Budiansky, J. W. Hutchinson, and J. C. Lambropoulos, Intl. J. Solids Struct. **19**, 337 (1983).

[42] A. G. Evans and R. M. Cannon, Acta Metall. **34**, 761 (1986).

[43] L. R. F. Rose, Proc. R. Soc. A **412**, 169 (1987).

[44] Q. P. Sun, K. C. Hwang, and S. W. Yu, J. Mech. Phys. Solids **39**, 507 (1991).

[45] T. Baxevanis, A. F. Parrinello, and D. C. Lagoudas, Int. J. Plasticity **50**, 158 (2013).

[46] C. Maletta and F. Furgiuele, Acta Mater. **58**, 92 (2010); C. Maletta and M. L. Young, J. Mater. Eng. Perform. **20**, 597 (2011); C. Maletta, Int. J. Fracture **177**, 39 (2012); C. Maletta, E. Sgambitterra, and F. Furgiuele, Fatigue & Fracture Eng. Mater. Struct. **36**, 903 (2013).

[47] P. M. Kelly and L. R. F. Rose, Progr. Mater. Sci. **47**, 463 (2002).

[48] S. D. Antolovich, Trans. Met. Soc. AIME **242**, 2371 (1968)

[49] R. M. McMeeking and A. G. Evans, J. Amer. Ceram. Soc. **65**, 242 (1982).

[50] N. Simha and L. Truskinovsky, Acta Metallurgica et Materialia **42**, 3827 (1994).

[51] V. M. Nabutovskii and B. Ya. Shapiro, Sov. Phys. JETP **48**, 480 (1978).

[52] A. L. Korzhenevskii, Sov. Phys. Solid State **28**, 745 (1986); **28**, 1999 (1986).

[53] A. Boulbitch and P. E. Pumpyan, Sov. Phys. Crystallogr. **35**, 156 (1990).

[54] A. Boulbitch and Yu. Gufan, Sov. Phys. JETP **67**, 1153 (1988); Ferroelectrics **98**, 277 (1989).

[55] A. Boulbitch and P. E. Pumpyan, Ferroelectrics **124**, 11 (1991); **111**, 111 (1990); J. Phys. I **3**, 1175 (1993); A. Boulbitch, V. P. Dmitriev, O. A. Zhelnova, and P. E. Pumpyan, Sov. Phys. JETP **71**, 619 (1990).

[56] A. A. Boulbitch and P. Toledano, Phys. Rev. Let. **81**, 838 (1998).

[57] A. A. Boulbitch, J. Mater. Sci. **27**, 1070 (1992).

[58] A. Boulbitch and A. L. Korzhenevskii, arXiv:1507.03128 (2015).

[59] V. I. Levitas, Int. J. Plasticity **16**, 805 (2000); **16**, 851 (2000); A. V. Idesman, V. I. Levitas, and E. Stein, *ibid.* **16**, 893 (2000).

[60] C. Bjerken and A. R. Massih, arXiv:1110.1292.

[61] A. Boulbitch and A. L. Korzhenevskii, Phys. Rev. Lett. **107**, 085505 (2011).

[62] A. Boulbitch and A. L. Korzhenevskii, Europhys. Lett. **112**, 16003 (2015).

[63] G. P. Cherepanov, *Mechanics of Brittle Fracture* (McGraw-Hill, New York, 1979).

[64] M. M. Vainberg and V. A. Trenogin, *Theory of Branching of Solutions of Non-Linear Equations* (Noordhoff, Leyden, 1974).

[65] Wolfram Research, Inc., MATHEMATICA, Version 10.0, Champaign, IL (2014).

[66] P. F. McMillan, Nat. Mater. **1**, 19 (2002); M. Kaczmarski, O. N. Bedoya-Martínez, and E. R. Hernández, Phys. Rev. Lett. **94**, 095701 (2005).

[67] M. Takeda, S. Ohnuki, P. R. Okamoto *et al.*, J. Electron Microsc. **48**, 609 (1999); K. Youssef, P. Kulshreshtha, and G. Rozgonyi, Photovoltaics for the 21st Century 5 **25**, 49 (2010); P. K. Kulshreshtha, K. M. Youssef, and G. Rozgonyi, Solar Energy Mater. Solar Cells **96**, 166 (2012).

[68] V. P. Sakhnenko and V. M. Talanov, Sov. Phys. Solid State **21**, 1401 (1979); **22**, 458 (1980).

[69] G. R. Barsch, T. Ohba, and D. M. Hatch, Mater. Sci. Eng. A **273-275**, 161 (1999); O. Shchyglo, U. Salman, and A. Finel, Acta Mater. **60**, 6784 (2012).

[70] E. Y. Tonkov, *High Pressure Phase Transformations: A Handbook* (Gordon and Breach, Amsterdam, 1992), Vols. 1–3; E. Y. Tonkov and E. G. Ponyatovsky, *Phase Transformations of Elements Under High Pressure* (CRC Press, Boca Raton, FL, 2005), Vol. 4.

[71] Yu. M. Gufan, *Structural Phase Transitions* (Nauka, Moscow, 1983) [in Russian].

[72] J. C. Toledano and P. Toledano, *The Landau Theory of Phase Transitions* (World Scientific, Singapore, 1987).

[73] P. R. Okamoto, N. Q. Lam, and S. Ohnuki, J. Electron Microsc. **48**, 481 (1999).

[74] L. E. Tanner, D. Schryvers, and S. M. Shapiro, Mater. Sci. Eng. **A127**, 205 (1990).

[75] K. Tozawa, Y. Haishi, Y. Matsukawa *et al.*, J. Electron Microsc. **48**, 613 (1999).